Mon. Not. R. Astron. Soc. **000**, 000–000 (0000) Printed June 9, 2015 (MN LaTeX style file v2.2)

Scaling of the 1-halo terms with bias

L. Raul Abramo[1⋆], Irène Balmès[1], Fabien Lacasa[2], Marcos Lima[1]
[1] *Departamento de Física Matemática, Instituto de Física, Universidade de São Paulo, CP 66318, CEP 05314-970 São Paulo, Brazil*
[2] *ICTP South American Institute for Fundamental Research, and Instituto de Física Teorica*
Universidade Estadual Paulista (UNESP), Rua Dr. Bento Teobaldo Ferraz 271, 01140-070 São Paulo, SP Brazil

June 9, 2015

ABSTRACT
In the Halo Model, galaxies are hosted by dark matter halos, while the halos themselves are biased tracers of the underlying matter distribution. Measurements of galaxy correlation functions include contributions both from galaxies in different halos, and from galaxies in the same halo (the so-called 1-halo terms). We show that, for highly biased tracers, the 1-halo term of the power spectrum obeys a steep scaling relation in terms of bias. We also show that the 1-halo term of the trispectrum has a steep scaling with bias. The steepness of these scaling relations is such that the 1-halo terms can become key contributions to the n-point correlation functions, even at large scales. We interpret these results through analytical arguments and semi-analytical calculations in terms of the statistical properties of halos.

Key words: cosmology: theory – large-scale structure of the Universe

1 INTRODUCTION

Galaxy surveys (York et al. 2000; Cole et al. 2005; Abbott et al. 2005; Scoville et al. 2007; Adelman-McCarthy et al. 2008a,b; PAN-STARRS; BOSS; Blake et al. 2011; Anderson et al. 2012, 2014) are not just tools for constraining cosmological parameters: they reveal the 3-dimensional spatial web of visible structures, the time evolution of these structures, and the history of galaxy evolution. Next generation astrophysical surveys are aimed at answering a variety of open astrophysical and cosmological questions, by collecting vast amounts of data from both galaxies and quasars, at low, intermediate, and high redshifts (BigBOSS; SUMIRE; Ellis et al. 2012; Abell et al. 2009; Benítez et al. 2009, 2014; Hill 2008).

For the study of how gravity and the Universe's background expansion affect the growth of structure, the standard statistical tools are the n-point correlation functions and their Fourier transforms, the polyspectra. If the distribution of matter were perfectly Gaussian, the two-point correlation function (2pCF) or, equivalently, the matter power spectrum, would contain all the statistical information. However, the primordial fluctuations are believed to be very nearly, but not perfectly, Gaussian. Information about the processes that generated these primordial perturbations is encoded in higher order moments, e.g. the bispectrum Maldacena (2003). Moreover, when subject to nonlinear time evolution, even a perfectly Gaussian initial field develops nontrivial higher-order moments (skewness, kurtosis, etc.) whereto statistical information propagates. At late stage of non-linear gravitational evolution, information even leaks out of the hierarchy of moments, as the density field becomes approximately lognormal (Carron 2011, 2012; Carron & Neyrinck 2012; Carron 2014).

Adding to these complications is the fact that we do not directly observe the total matter distribution, but only its visible component — which accounts to $\sim 20\%$ of the total matter (see, e.g. Planck Collaboration 2015) and is affected by non-gravitational effects such as the physics of baryons, radiation pressure, feedback, etc. Hence, the 2pCF of the distribution of visible matter cannot possibly tell the full story and we must treat galaxies, quasars, Ly-α systems, etc., as unfaithful (and biased) tracers of the underlying dark matter (DM) distribution.

The relation between tracers of large-scale structure (LSS) and the DM distribution is partially provided by the Halo Model (Cooray & Sheth 2002). The DM halos — and not the DM particles — then become the fundamental objects. In particular, the correlation functions of the DM halos are related to the correlation functions of the DM particles by the halo abundance, bias and profile, such that more massive halos are less abundant, are more highly biased and have less concentrated profiles.

The statistics of how galaxies populate DM halos is provided by the so-called Halo Occupation Distribution (HOD) (Cooray & Sheth 2002; Martinez & Saar 2001; Berling & Weinberg 2002; Kravtsov et al. 2003; Zheng et al. 2005). Galaxies inhabiting more massive halos typically have a higher bias. HOD parameters can be calibrated by measurements of specific abundance ratios, and by matching the

⋆ abramo@if.usp.br

correlation functions of the tracers to those expected from the Halo Model.

The relationship between the statistics of the DM density field and that of galaxies is often non-trivial. For example, the n-point statistics of galaxies get contributions from the N-halo term (when each galaxy occupies a different halo), from the $(N-1)$-halo term (when two galaxies occupy the same halo, and the others lie in different halos), etc., all the way down to the 1-halo term (when all the N galaxies occupy the same halo). Furthermore, there are contributions to the N-point statistics from $N-1$ types of shot-noise terms: e.g., the $(N-1)$-halo – $(N-1)$-galaxy term (when the correlation function hits twice a galaxy in a given halo, and then only once galaxies in different halos) down to the 1-halo – 1-galaxy term (when the correlation function hits N times the same galaxy). Hence, when we measure the N-point function of galaxies, we are in fact measuring an ad-mixture of all the N'-point functions of halos ($N' = 1, 2, \ldots, N$).

The measurement of the galaxy 2pCF includes both a 2-halo term (related to galaxies in two distinct halos) and a 1-halo term (accounting for galaxies within the same halo). Clearly, the 2-halo term is most important on large scales, near the linear regime, and bears the imprint of the large-scale matter distribution, whereas the 1-halo term dominates on small, nonlinear scales, and reflects the matter distribution inside halos (the halo profile). Even though these two regimes are connected by time-evolution, we may describe the galaxy power spectrum as the superposition of two independent scaling laws: that of the linear DM power spectrum, which dominates on large scales, and that coming from the halo profiles, which dominates on small scales ($k \gtrsim 1\, h$ Mpc^{-1}).

In the large-scale limit the 1-halo term contributes a constant to the galaxy power spectrum. This constant may be poorly known, since galaxy surveys designed for cosmological studies are often insufficiently complete (or have poor redshift accuracy, in case of photometric redshifts) to determine precisely the HOD parameters for a type of galaxy, and for the survey's mean redshift. This constant represents a noise that must be subtracted from the power spectrum — just as it happens with shot noise, which has a completely different origin but is also a constant that must be subtracted. This feature of the 1-halo term on large scales also comes into play in higher-order statistics: the bispectrum gets a constant contribution from the 1-halo term of the 3-point function; the trispectrum gets a constant contribution from the 1-halo term of the 4-point function; and so on.

In this paper we study the behavior of the 1-halo terms as a function of bias, where these quantities are connected via their mutual dependence on HOD parameters. The same goes for the other observable quantities, such as the mean number density of galaxies, the 2-halo term of the power spectrum, etc. Hence, the HOD provides an internal (but unobservable) parameter space that we can use to vary the observable quantities. In particular, we use bias to parametrize the 1-halo terms both because it is more readily available in observations, and also because we are interested in identifying universal behaviors, regardless of the details of the HODs.

We show that, for highly biased tracers ($b_g \gtrsim 3$), the 1-halo term of the 2pCF obeys a scaling relation in terms of bias, growing as $P^{1h} \sim b_g^{4-5}$, which is much faster than the scaling of the 2-halo term ($P^{2h} = b_g^2 P_m$, where P_m is the matter power spectrum). For highly biased galaxies, the effective shot noise contributed by the 1-halo term can become at least comparable to Poisson shot noise, significantly lowering the signal-to-noise ratio for measurements of the power spectrum, baryon acoustic oscillations, etc. In some cases the 1-halo term can even surpass by a large factor the shot noise, as is the case, e.g., for the angular power spectrum of the cosmic infrared background on the angular scales probed by Herschel Thacker et al. (2013). Furthermore, we show that the 1-halo term for the trispectrum also grows very fast — typically, like $(P^{1h})^3$ — and should, therefore, contribute an important source of noise for the power spectrum covariance in the limit of high bias.

When employing a particular cosmological model below, we used a standard flat ΛCDM scenario, with $\Omega_m = 0.26$, $n_s = 0.96$ and $\sigma_8 = 0.78$.

2 FORMALISM AND ANALYTICAL APPROXIMATIONS

2.1 The Halo Model

Over time, gravity enhances the density contrast field by attracting matter towards the density peaks, and by creating voids where the density was initially below-average. The Halo Model (Cooray & Sheth 2002) describes how this process evolves over time, by determining e.g. the abundances of the DM halos as function of their masses and redshifts — i.e., the mass function, $d\,\bar{n}_h/d\log M$.

Halos are ultimately determined by the peaks of the initial density field, and according to the theory of peak statistics (Bardeen et al. 1986; Mo & White 1996), the main driver of the abundance of peaks as a function of mass is the mass variance within a certain comoving radius R. The variance of the linear density field inside a spherical top-hat region of radius R is determined by:

$$\begin{aligned} \sigma^2(R) &= \frac{1}{2\pi^2}\int dk\, k^2 P_m(k) W(kR) \\ &= \int d\ln k\, \Delta_m^2(k) W(kR)\,, \end{aligned} \tag{1}$$

where $P_m(k)$ is the linear matter power spectrum and $W(x) = [3j_1(x)/x]^2$ is the window function for a spherical top-hat region. The mass contained within radius R at the mean background matter density today is $M(R) = 4\pi R^3 \bar{\rho}_m/3$. The peak height is defined as $\nu(M) = \delta_c/\sigma(M)$, where δ_c is the linearly extrapolated critical density contrast for spherical collapse.

Due to the statistics of density peaks (Bardeen et al. 1986), all mass functions exhibit an exponential dependence on the peak height $\nu(M)$. In fact, we can write:

$$\frac{d\bar{n}_h}{d\ln M} = \frac{\rho_m}{M}\frac{d\ln\sigma^{-1}}{d\ln M} f(\nu)\,, \tag{2}$$

where, up to some model-dependent factors and coefficients, $f(\nu) \sim e^{-\nu^2/2}$.

Another crucial ingredient of the Halo Model is the halo bias. Since we would like to substitute the true matter density contrast δ_m by the contrast of halo counts,

$\delta_h = n_h/\bar{n}_h - 1$, a relationship between the two must be established. We can write this in terms of a local ansatz such as Fry & Gaztañaga (1993):

$$\delta_h = b_h \delta_m + b_h^{(2)} (\delta_m^2 - \sigma_m^2) + \cdots \, . \quad (3)$$

In this paper we will only consider the first term in this relation — the higher-order terms can also become important precisely in the limit that we are investigating (tracers with high bias), but we leave this key issue for future investigations. Typically, halo bias is a smooth power-law function of peak height, such that more massive halos correspond to higher (and rarer) peaks and have higher values of the halo bias.

Our analytical calculations were performed using both the Press-Schechter (Press & Schechter 1974) (PS) as well as the Sheth-Tormen (Sheth & Tormen 1999; Sheth, Mo & Tormen 1999) (ST) prescriptions for the mass function and halo bias. Our semi-analytical calculations were performed using the Tinker mass function (Tinker et al. 2008) and halo bias (Tinker et al. 2010). The main results are very similar on all cases.

2.2 Halo Profile

Related to the Halo Model, but still a slightly orthogonal result which depends more strongly on the non-linear regime of structure formation, is the shape of the halo profiles. Although our results are completely insensitive to the fine details of these profiles, in our semi-analytical calculations we employ the standard results of Navarro, Frenk & White (1997). In that case, the density profile for a halo of mass M is given by:

$$\rho(r|M) \sim u(r|M) \sim \frac{1}{\frac{r}{r_s}\left(1+\frac{r}{r_s}\right)^2} \, , \quad (4)$$

where $r_s = r_s(M)$ is the characteristic scale ("knee") for a halo of mass M. The mass-averaged halo profile in Fourier space is computed as:

$$u(k|M) = \frac{4\pi}{M} \int dr \, r^2 \, \frac{\sin kr}{kr} \, \rho(r|M) \, . \quad (5)$$

The important feature for our purpose is that $u(k|M) \to 1$ when $k \lesssim 1 \, h$ Mpc^{-1} for the range of masses that we are interested in.

Here we are implicitly assuming that the profile of the galaxy counts is identical to the DM density profile. This may not be true, especially at the innermost regions of the DM halos, where the galaxy profiles seem to be significantly steeper than the NFW profile (Watson et al. 2010; Kayo & Oguri 2012; Piscionere et al. 2014). Nevertheless, the property that $u(k) \to 1$ for $k \lesssim 1 \, h$ Mpc^{-1} follows simply from the fact that $u(k \to 0) = (1/M) \int d^3x \, \rho = 1$, so it remains valid for all relevant profiles.

2.3 Halo Occupation Distribution

It has been known for a long time that there must be a direct relation between the distribution of galaxies and that of the underlying dark matter halos (White & Frenk 1991; Kauffmann, White & Guideroni 1993; Navarro, Frenk & White 1995; Mo & White 1996; Kauffmann et al. 1999; Springel et al. 2005). Halo Occupation Distribution (HOD) models provide the probability distribution function $P(N|M)$ for a certain number (N) of galaxies to occupy halos of a given mass (M) (Ma & Fry 2000; Seljak 2000; Cooray & Sheth 2002; Martinez & Saar 2001; Berling & Weinberg 2002; Zheng et al. 2005). Although halo mass is not the only factor which determines richness (Zentner, Hearin & van den Bosch 2014), HODs have been extremely useful to interpret measurements of the clustering of different types of tracers, from galaxies (Zheng, Coil & Zehavi 2007; Zheng et al. 2009) to quasars (Porciani, Magliocchetti, & Norberg 2004; Shen et al. 2007; Wake et al. 2008; Shen et al. 2010; Kayo & Oguri 2012; Richardson et al. 2012) — however, in the latter case the simplest HODs may be inadequate to capture the complex interactions between quasars and their environments (Shen et al. 2013; Chatterjee et al. 2013; Cen & Safarzadeh 2015), and additional parameters such as assembly bias should be included. Often, instead of $P(N|M)$, what is provided are the momenta of the HOD, such as $\bar{N}(M) = \langle N \rangle_M$, $\langle N(N-1) \rangle_M$, etc., or even the conditional probabilities. The brackets define averages are over halos of the same mass, and the HOD can be defined in terms of the momenta (we will drop the subscript M from now on, for brevity).

It is clear that, for very massive halos, the number of tracers should scale proportionally to halo mass, but as we approach the low-mass end the situation can be more nuanced. According to the hierarchical scenario of structure formation, a galaxy can either form inside its original halo, or it can join an already existing, populated halo, at a later time. Hence, it is useful to distinguish "central" galaxies, of which there can be only one per halo, and "satellites", whose distributions may be quite different as a function of halo mass. A popular functional form for the richness of central and satellite galaxies is (see, e.g., Zheng et al. (2005)):

$$\langle N_c \rangle \;=\; \bar{N}_c = \frac{1}{2} \, \mathrm{Erfc} \left(\frac{M_c - M}{\sqrt{2} \, \sigma_g} \right) \quad (6)$$

$$\langle N_s \rangle \;=\; \bar{N}_s = \bar{N}_c \times \tilde{N}_s \, , \quad (7)$$

where:

$$\tilde{N}_s = \theta(M - \kappa_g M_c) \left(\frac{M - \kappa_g M_c}{M_1} \right)^\alpha \, . \quad (8)$$

As denoted by Eq. (7), the existence of satellites is conditional on the existence of a central galaxy. Typical values for the HOD parameters are $M_c \simeq 10^{13.5} \, h^{-1} \, M_\odot$, $M_1 \simeq 10^{14} \, h^{-1} \, M_\odot$, $\alpha \simeq 0.9 - 1.0$, $\kappa_g \simeq 1.1$, $\sigma_g \simeq 1$ (Zheng et al. 2005) — although, in the case of quasars, especially at high redhifts, some parameters can deviate significantly from these values (Chatterjee et al. 2013).

Besides the mean numbers (or richness), we must also specify the higher-order momenta of $P(N, M)$. If we are only interested in the 2-halo and in the 1-halo terms, then all we need are the expectation values $\langle N_c^2 \rangle$, $\langle N_c N_s \rangle$ and $\langle N_s^2 \rangle$. The model separating central and satellite galaxies naturally provides these momenta. By definition, the central galaxy either exists ($N_c = 1$) or does not exist ($N_c = 0$) inside a halo so $\langle N_c(N_c - 1) \rangle = 0$ or equivalently $\langle N_c^2 \rangle = \bar{N}_c$. Regarding the cross-correlation between central satellite galaxies, notice that satellites can only exist if there is already at least one central galaxy, so $\langle N_c N_s \rangle = \bar{N}_s$. As for the satellites, we can assume a simple Poisson distribution, which means, in particular, that $\langle N_s^2 \rangle = \bar{N}_s(\tilde{N}_s + 1)$.

2.4 Combining the Halo Model and the HOD

The Halo Model allows us to compute several quantities of interest from these ingredients. The mean galaxy number density is:

$$\bar{n}_g = \int d\ln M \frac{d\bar{n}_h}{d\ln M} \times \bar{N}(M) \; , \tag{9}$$

where $\bar{N} = \bar{N}_c + \bar{N}_s$. The galaxy bias is given by:

$$b_g(k) = \frac{1}{\bar{n}_g} \int d\ln M \frac{d\bar{n}_h}{d\ln M} \times \bar{N}(M) b(M) u(k|M) \; , \tag{10}$$

where recall that $u(k|M) \to 1$ for $k \lesssim 1\, h$ Mpc^{-1}. In terms of the galaxy bias, the two-halo galaxy power spectrum is given by:

$$P^{2h}(k) = b_g^2(k) P_m(k) \; . \tag{11}$$

The 1-halo term, on the other hand, is given by:

$$\begin{aligned} P^{1h}(k) &= \frac{1}{\bar{n}_g^2} \int d\ln M \frac{d\bar{n}_h}{d\ln M} \times \langle N(N-1) \rangle \, |u(k|M)|^2 \\ &= \frac{1}{\bar{n}_g^2} \int d\ln M \frac{d\bar{n}_h}{d\ln M} \\ &\quad \times \bar{N}_c(M) \left[2\tilde{N}_s(M) + \tilde{N}_s^2(M) \right] |u(k|M)|^2 \; , \end{aligned} \tag{12}$$

where the term inside square brackets in the second line is the intra-halo number variance, given the assumptions outlined above.

The measured galaxy power spectrum is therefore:

$$P_g = P^{2h} + P^{1h} + P_S \; , \tag{13}$$

where P_S is the shot noise power spectrum — which, under the assumption of Poissonian statistics for the galaxy counts, is given by $P_S = 1/\bar{n}_g$.

Similar arguments can also be applied to higher-order correlations, such as the 4-point function, or in Fourier space to the trispectrum $T(\vec{k}_1, \vec{k}_2, \vec{k}_3, \vec{k}_4)$. In particular, the trispectrum determines the covariance of the two-point function – i.e., the power spectrum – in the form $T(\vec{k}, -\vec{k}, \vec{k}', -\vec{k}')$. The 1-halo term of this part of the trispectrum is given by:

$$\begin{aligned} T_g^{1h}(\vec{k}, -\vec{k}, \vec{k}', -\vec{k}') &= \frac{1}{\bar{n}_g^4} \int d\ln M \frac{d\bar{n}_h}{d\ln M} \\ &\quad \times \langle N(N-1)(N-2)(N-3) \rangle \\ &\quad \times |u(k|M)|^2 \, |u(k'|M)|^2 \\ &= \frac{1}{\bar{n}_g^4} \int d\ln M \frac{d\bar{n}_h}{d\ln M} \\ &\quad \times \bar{N}_c [4\tilde{N}_s^3 + \tilde{N}_s^4] \\ &\quad \times |u(k|M)|^2 \, |u(k'|M)|^2 \; , \end{aligned} \tag{14}$$

where on the second line of the equation above we used the same assumptions about the statistics of central and satellite galaxies that were used to obtain the expression in the second line of Eq. (12).

For our purposes, we will consider scales larger than the sizes of the largest halos, so we take $u(k|M) \to 1$ in all our expressions from now on. We have checked that this is an excellent approximation for $k \lesssim 1\, h$ Mpc^{-1}.

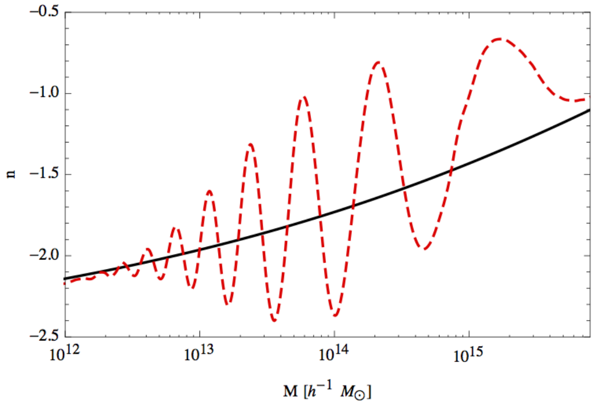

Figure 1. Power-law index as a function of M. Solid (black) line: $n = -3(1 + d\ln\sigma^2/d\ln M)$. Dashed (red) line: $n_P = d\ln P(k)/d\ln k$, evaluated at $k = k_R = 1/R(M)$. The wiggles seen in n_P are caused by the BAOs.

2.5 Analytical model for the peak height

In some of the following subsections we will perform analytical computations of several quantities of interest in the PS (Press & Schechter 1974) and ST (Sheth & Tormen 1999; Sheth, Mo & Tormen 1999) formalisms. In order to carry out those calculations we need an analytical approximation for the peak height in terms of the halo mass.

The variance of the linear density field inside a tophat spherical region of radius R was given in Eq. (1). Since the spherical tophat window function has the features that $W(0) = 1$ and $W \to 0$ for $x \gg 1$, with a full width at half maximum of approximately $x_{FWHM} \approx 1$, it is fair to approximate the variance as:

$$\sigma^2(R) \approx \Delta_m^2(k = k_R) \propto k_R^3 \, P_m(k_R) \; , \tag{15}$$

where $k_R = 1/R$. For self-similar models in which $P_m(k) \propto k^n$, we have $\sigma^2(R) \propto k_R^{n+3} \propto R^{-(n+3)}$. In terms of the mass contained inside radius R at the mean background density, $M \propto R^3$, we have:

$$\sigma^2(M) \propto M^{-(n+3)/3} \; . \tag{16}$$

Even though LSS in a standard ΛCDM Universe is not described by a self-similar model, it will be useful to consider this case as it will allow us to obtain interesting analytical expressions for fixed n.

The peak height, normalized to 1 at $M = M^*$, is given by:

$$\nu = (M/M_*)^{(n+3)/6} \; , \tag{17}$$

where M_* is typically $\sim 2. \times 10^{13}\, h^{-1}\, M_\odot$ in the ΛCDM models. In particular, within this approximation we have $d\ln\sigma^{-1}/d\ln M = (n+3)/6$.

We check the approximation of Eq. (16) in Fig. 1, where we plot the power-law index $n = -3(1 + d\ln\sigma^2/d\ln M)$ (solid, black line) together with $n_P = d\ln P(k)/d\ln k$, evaluated at $k = k_R = 1/R(M)$ (dashed, red line). The slope of the power spectrum, n_P, shows the wiggles from the BAOs. The power index of the peak height, on the other hand, is an average over several different scales, hence it is only sensitive to the mean slope of the power spectrum. It is clear that the two are closely related, and that the approximation of Eq. (17) holds quite well for n between -2 and -1 in the mass range considered. In Sections 3.3 and 3.4 we do not use this approximation anymore, and instead compute $\sigma(M)$ from the power spectrum in a ΛCDM model.

2.6 Mass functions and halo bias

The simplest case is that of the Press-Schechter (PS) formalism (Press & Schechter 1974). It provides closed-form expressions for the mass function and halo bias:

$$f_{PS}(\nu) = \sqrt{\frac{2}{\pi}}\nu \exp\left[-\nu^2/2\right] , \tag{18}$$

$$b_{PS}(\nu) = 1 + \frac{\nu^2 - 1}{\delta_c} . \tag{19}$$

These formulas are in poor agreement with the data and N-body simulations, however, when used in conjunction with an extremely simple HOD, they yield simple, straightforward analytical calculations whose results convey the basic message of this paper — see Section 3.1.

A better fit to simulations and observations is given by the ST mass function and halo bias (Sheth & Tormen 1999; Sheth, Mo & Tormen 1999):

$$f_{ST} = A\sqrt{\frac{2a}{\pi}}\left[1 + (a\nu^2)^{-p}\right] \nu\, e^{-a\nu^2/2} , \tag{20}$$

$$b_{ST} = 1 + \frac{a\nu^2 - 1}{\delta_c} + \frac{2p}{\delta_c[1 + (a\nu^2)^p]} , \tag{21}$$

where $A \simeq 0.322$, $a \simeq 0.71$, and $p \simeq 0.3$. The ST framework gives a more accurate description compared to PS, while still allowing for fully analytical calculations. In Section 3.2 we use the ST formulas and a slightly more realistic HOD compared with the calculation in the PS case — yet the main results of that Section are basically unchanged.

Finally, we also consider the expressions found by Tinker et al. (2008, 2010), which were calibrated from numerical simulations. The mass function Tinker et al. (2008) and bias Tinker et al. (2010) are given in this case by:

$$f(\sigma) = 0.186 \times \left[\left(\frac{\sigma}{2.57}\right)^{-1.47} + e^{-1.2/\sigma^2}\right] , \tag{22}$$

$$b_h(\nu) = 1 - A_T\frac{\nu^{a_T}}{\nu^{a_T} + \delta_c^{a_T}} + B_T\nu^{b_T} + C_T\nu^{c_T} , \tag{23}$$

where $A_T = 1 + 0.24\, y \exp[-(4/y)^4]$ (with $y = \log_{10}\Delta$, where we choose $\Delta = 200$), $a_T = 0.44\, y - 0.88$, $B_T = 0.183$, $b_T = 1.5$, $C_T = 0.019 + 0.107\, y + 0.19 \exp[-(4/y)^4]$, and $c_T = 2.4$. We will employ this mass function in our semi-analytical calculations, assuming now a realistic HOD — see Section 3.3. As we shall see shortly, the results are qualitatively identical to those of Sections 3.1 and 3.2, which were found by means of analytical calculations.

3 APPLICATIONS

3.1 Press-Schechter mass function and a simple HOD

We begin assuming an extremely simplified HOD, which should hold in an approximate sense for sufficiently high halo masses (see, e.g., Porciani, Magliocchetti, & Norberg (2004)):

$$\bar{N}(M) = \left(\frac{M}{M_1}\right)^{\alpha} \theta(M - M_1) , \tag{24}$$

where $\theta(x)$ is the Heaviside step-function. In this simple HOD we take the cut-off mass to be equal to the mass scale M_1. This HOD also assumes that all galaxies are satellites. In the final subsections we recover the full description in terms of $\bar{N}_c$ and $\bar{N}_s$, and show that the central galaxies are unimportant in the limit we are interested in ($b_g \gtrsim 3$). Except for the low-mass limit, the halo richness should scale roughly proportional to its mass, so $\alpha \approx 1$. We will assume for the moment that M_1 also defines the threshold for finding galaxies in halos – i.e., $\bar{N} = 0$ for $M < M_1$. This approximation will be improved in the next subsection, where we carry out the same calculations as here, but using the Sheth-Tormen formalism. As we will see, this does not change significantly our main results.

We start by computing the number density of halos which host at least one galaxy in our simple HOD, Eq. (24). Since the number of galaxies in each halo follows a Poisson distribution, this is given by:

$$\bar{n}_{h/g} = \int d\ln M \frac{d\bar{n}_h}{d\ln M}\left[1 - \exp(-\bar{N})\right] \tag{25}$$

Another definition, which will become more useful later on, is the number of halos that *could* contain galaxies:

$$\begin{aligned}\bar{n}_{h,g} &= \int_{M_1}^{\infty} d\ln M \frac{d\bar{n}_h}{d\ln M} \\ &= \int_{M_1}^{\infty} d\ln M\, \frac{\rho_m}{M}\frac{d\ln\sigma^{-1}}{d\ln M}\sqrt{\frac{2}{\pi}}\nu \exp\left[-\nu^2/2\right] \\ &= \sqrt{\frac{2}{\pi}}\frac{\rho_m}{M_*}\int_{\nu_1}^{\infty} d\nu\, \nu^{-6/(n+3)} e^{-\nu^2/2} ,\end{aligned} \tag{26}$$

where we have used the PS mass function and the approximations $M = M_*\nu^{6/(n+3)}$, as well as the definition $\nu_1 = (M_1/M_*)^{(n+3)/6}$.
For high M_1 the integral in Eq. (25) is dominated by the exponential behavior of the mass function, and we can replace the $\bar{N}$ in the exponent by the mean number of galaxies in the halos just above the cut-off mass scale, $\bar{N}(M) \to \bar{N}(M_1) = \bar{N}_{\rm min}$. Hence, the actual number of halos containing galaxies can be approximated by $\bar{n}_{h/g} \approx (1 - e^{-\bar{N}_{\rm min}}) \times \bar{n}_{h,g}$. For the HOD of Eq. (24) this minimum mean number of galaxies is $\bar{N}_{\rm min} = 1$, so $\bar{n}_{h/g} \approx 0.63\, \bar{n}_{h,g}$.

With the variable change $x \equiv \nu^2/2$ we obtain:

$$\bar{n}_{h,g} = \sqrt{\frac{2}{\pi}}\frac{\rho_m}{M_*}2^{\lambda_0}\int_{x_1}^{\infty} dx\, x^{\lambda_0} e^{-x} = \sqrt{\frac{2}{\pi}}\frac{\rho_m}{M_*}2^{\lambda_0}\Gamma(1+\lambda_0, x_1) , \tag{27}$$

where $\lambda_0 = -1/2 - 3/(n+3)$, $x_1 = \nu_1^2/2$, and $\Gamma(\kappa, x)$ is the (upper) incomplete Gamma function of order κ. Typically, $-2 \lesssim n \lesssim -1$ for halos at the scales of interest, which means that $-7/2 \lesssim \lambda_0 \lesssim -2$.

The incomplete Gamma function is related to the simple Gamma function by $\Gamma(\kappa) = \Gamma(\kappa, x = 0)$, and has asymptotic limits given by:

$$\lim_{x\to 0} \Gamma(\kappa, x) \;\to\; \Gamma(\kappa) - x^{\kappa}\left[\frac{1}{\kappa} - \frac{x}{1+\kappa} + \mathcal{O}(x^2)\right] , \tag{28}$$

and

$$\lim_{x\to\infty} \Gamma(\kappa,x) \;\to\; e^{-x}\,x^{\kappa-1}\left[1+\frac{\kappa-1}{x}+\mathcal{O}(x^{-2})\right] \,. \quad (29)$$

Notice, in particular, that $\lim_{x\to\infty}\Gamma(1+\kappa,x)/\Gamma(\kappa,x)\to 1+x+\mathcal{O}(x^{-1})$. It is also interesting to note that, for $0\lesssim\kappa\lesssim 1$, the asymptotic expression of Eq. (29) is remarkably accurate down to $x\simeq 1$.

Hence, for the ranges of interest for n, in which λ_0 is negative, the number density of the halos that host galaxies should diverge in the limit $x_1\to 0$ — i.e., when $M_1 \ll M_*$. Indeed, the number of halos of arbitrarily small masses is arbitrarily large, unless we specify a smoothing scale R_f, in which case it asymptotes to $\bar{n}_{h,g}\propto R_f^{-3}$ (Bardeen et al. 1986).

Similarly as was done above, we can compute other quantities of interest analytically. For the mean number density of galaxies we obtain:

$$\begin{aligned}\bar{n}_g &= \int_{M_1}^{\infty} d\ln M\,\frac{d\bar{n}_h}{d\ln M}\times\bar{N}(M) \quad (30)\\ &= \sqrt{\frac{2}{\pi}}\frac{\rho_m}{M_*}\left(\frac{M_*}{M_1}\right)^{\alpha} 2^{\lambda_1}\Gamma(1+\lambda_1,x_1)\,,\end{aligned}$$

where we have used the same definitions as above, with the difference that now the index is $\lambda_1=\lambda_0+3\alpha/(n+3)=-1/2+3(\alpha-1)/(n+3)$. Since $\alpha\simeq 1$ and $-2\lesssim n\lesssim -1$, we have $\lambda_1\simeq -1/2$. Notice that for the case $\alpha=1$, $\lambda_1=-1/2$ and in the limit $x_1\to 0$, we have $\bar{n}_g=\rho_m/M_1=\rho_m\langle N\rangle/M$

Interestingly, using Eq. (29) we find that in the high mass limit ($x_1\to\infty$), $\bar{n}_g=\bar{n}_{h,g}$ – i.e., in that case the number of halos that could host a galaxy is equal to the mean number of galaxies. This is a consequence of the simple HOD, Eq. (24), which takes the cut-off mass to be identical to the mass scale M_1. Since the galaxy bias increases with M_1, for high values of this mass the number of halos above the cut-off is exponentially suppressed, and only the least massive halos are populated with galaxies. In this case each halo ends up hosting only one galaxy — or, more accurately, because of Poisson statistics, about 63% of halos contain only one galaxy, and the rest contain two or more galaxies.

We can calculate the galaxy bias in the same fashion, using the PS halo bias of Eq. (19):

$$b_g = 1-\delta_c^{-1}+2\delta_c^{-1}\frac{\Gamma(2+\lambda_1,x_1)}{\Gamma(1+\lambda_1,x_1)}\,. \quad (31)$$

In the $x_1\to 0$ limit we can use the property of the Gamma function $\Gamma(2+\lambda_1)=(1+\lambda_1)\Gamma(1+\lambda_1)$, which leads to $b_g\simeq 1-\delta_c^{-1}+2\delta_c^{-1}(1+\lambda_1)$. We also note that taking $\alpha=1$ leads to $\lambda_1=-1/2$ and $b_g=1$, simply reflecting the halo bias consistency relation. On the other hand, in the limit of very large threshold masses ($x_1\gg 1$) we obtain $b_g\simeq 1+\delta_c^{-1}+2\delta_c^{-1}x_1$. Hence, in order to increase bias, it is sufficient that $x_1\gg 1$ — however, this is not a necessary condition: one could also fix the cut-off mass scale and decrease n, or increase α.

A similar calculation as the one performed in Eq. (30) leads to an expression for the 1-halo term of the galaxy power spectrum:

$$\begin{aligned}P^{1h} &= \frac{1}{\bar{n}_g^2}\int d\ln M\,\frac{d\bar{n}_h}{d\ln M}\bar{N}^2\\ &= \left[\sqrt{\frac{2}{\pi}}\frac{\rho_m}{M_*}2^{2\lambda_1-\lambda_2}\right]^{-1}\times\frac{\Gamma(1+\lambda_2,x_1)}{[\Gamma(1+\lambda_1,x_1)]^2}\,, \quad (32)\end{aligned}$$

where on the first line the term $\langle N(N-1)\rangle$ reduces to $\bar{N}^2$ since we only have satellite galaxies with a Poisson distribution, and on the second line we have substituted the expression for $\bar{n}_g$ and $\lambda_2=\lambda_0+6\alpha/(n+3)$. Using the expression for the number density of halos hosting these galaxies, Eq. (26), we obtain:

$$P^{1h}=\frac{\Gamma(1+\lambda_0,x_1)\,\Gamma(1+\lambda_2,x_1)}{[\Gamma(1+\lambda_1,x_1)]^2}\times\frac{1}{\bar{n}_{h,g}}\,. \quad (33)$$

Notice that the three indices, λ_0 (that appeared in $\bar{n}_{h,g}$), λ_1 (which appeared in $\bar{n}_g$ and b_g), and λ_2, are related by $\lambda_0=2\lambda_1-\lambda_2$. By substituting the asymptotic expression for $\Gamma(\kappa,z)$ in the limit $z\to\infty$ one can verify that the prefactor appearing Eq. (33) is $\Gamma(1+\lambda_0,x_1)\Gamma(1+\lambda_1,x_1)/[\Gamma(1+\lambda_1,x_1)]^2\simeq 1$. Hence, in the limit of high threshold mass, $P^{1h}\approx 1/\bar{n}_{h,g}$.

In the opposite limit, of low threshold masses, the prefactor can become quite large — but then so does $\bar{n}_{h,g}$ become large. In general, this case corresponds to tracers with low biases. In that limit, it is convenient to revert to the original expression, Eq. (32), and write instead:

$$\begin{aligned}P^{1h} &= \frac{2^{\lambda_2-\lambda_1}}{\bar{n}_g}\left(\frac{M_*}{M_1}\right)^{\alpha}\frac{\Gamma(1+\lambda_2,x_1)}{\Gamma(1+\lambda_1,x_1)} \quad (34)\\ &\simeq \frac{2^{\lambda_2-\lambda_1}}{\bar{n}_g}\left(\frac{M_*}{M_1}\right)^{\alpha}\frac{\Gamma(1+\lambda_2)}{\Gamma(1+\lambda_1)}\,.\end{aligned}$$

Let us suppose that we can change the HOD parameters while maintaining the mean number of galaxies, $\bar{n}_g$, fixed. In the limit of low-mass threshold the bias is $b_g\approx 1-\delta_c^{-1}+\delta_c^{-1}[1+6(\alpha-1)/(n+3)]$ — i.e., higher values of α and/or lower values of n correspond to higher biases. Since $\lambda_2=\lambda_1+3\alpha/(n+3)$, the ratio of Gamma functions in Eq. (34) can be regarded as a steep function of bias.

From Eq. (33) we see that P^{1h}, which is proportional to $1/\bar{n}_{h,g}$, plays the role of a *halo* shot noise term. For highly biased tracers (whose mass thresholds are relatively high), the galaxies end up in just a few halos, so that the halo shot noise term becomes an important part of the power spectrum and its covariance. This means, in particular, that the barrier for measuring the (2-halo) power spectrum with highly biased tracers may not be just the shot noise of that tracer, but also an additional *halo shot noise* coming from the 1-halo term.

In the limit of high bias (and high mass thresholds) we can neglect the subdominant dependence in the prefactor of $1/\bar{n}_{h,g}$ in Eq. (33), and express the contribution of the halo shot noise term as a function of bias. Using $b_g\simeq 1+\delta_c^{-1}+2\delta_c^{-1}x_1\to 2\delta_c^{-1}x_1$, the mean number density of halos can be expressed as:

$$\bar{n}_{h,g}\sim x_1^{-\frac{n+9}{2(n+3)}}\,e^{-x_1}\sim b_g^{-\frac{n+9}{2(n+3)}}\,e^{-b_g\,\delta_c/2}\,, \quad (35)$$

hence:

$$P^{1h}\sim x_1^{\frac{n+9}{2(n+3)}}\,e^{x_1}\sim b_g^{\frac{n+9}{2(n+3)}}\,e^{b_g\,\delta_c/2}\,. \quad (36)$$

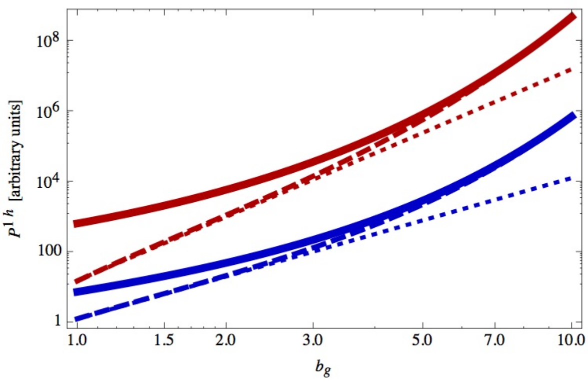

Figure 2. Scaling of the 1-halo term in the PS model. The exact formula, Eq. (32), is denoted by the thick solid lines (upper line: $n = -2$; lower line: $n = -1$), while the dashed lines correspond to the approximation of Eq. (36). The dotted lines are the power laws b_g^4 (for the case $n = -1$) and b_g^6 (for the case $n = -2$).

For intermediate values of the galaxy bias the 1-halo term is well approximated by a power-law. In Fig. 2 we show the exact formula, Eq. (32), for the cases $n = -1$ (lower solid line) and $n = -2$ (upper solid line), in arbitrary units. The first approximation in the middle of Eq. (36) is plotted as the dashed lines for the two cases, where we used $x_1 \approx (1 - \delta_c + \delta_c\, b_g)/2$. One can see that the approximation becomes better for higher values of the bias. Also plotted (dotted lines) are the power laws b_g^4 (for the case $n = -1$) and b_g^6 (for the case $n = -2$). The simple power laws shown in Fig. 2 are a good approximation in the interval $1.5 \lesssim b_g \lesssim 3$.

Since the 2-halo term scales as $P^{2h} = b_g^2\, P_m$, but the 1-halo term grows much faster with bias, the latter component should become increasingly important for highly-biased tracers. In fact, this already happens at small scales ($k \gtrsim 1\ h$ Mpc^{-1}) even for galaxies with relatively low biases. If we select tracers with increasing values of the bias (e.g. quasars), the 1-halo term will become more important, even in the large-scale limit, acting effectively as a type of "halo shot noise". However, in contrast to the usual situation where shot noise can be beaten down by observing a larger number of galaxies, when the tracers are very highly biased this halo shot noise cannot be lowered, and a limiting factor for measuring the power spectrum is the finite number of halos, and not only the number of galaxies in the survey.

It is easy to see that this argument also applies to higher-order correlation functions. The same type of integral computed above appears also in the 1-halo term of the trispectrum, Eq. (14), and taking $k \to 0$ and $k' \to 0$ leads to:

$$\begin{aligned} T^{1h} &= \frac{1}{\bar{n}_g^4} \int d\ln M\, \frac{d\bar{n}_h}{d\ln M} [4\bar{N}^3 + \bar{N}^4] \\ &= \frac{1}{\bar{n}_g^4} \times \sqrt{\frac{2}{\pi}} \frac{\rho_m}{M_*} \left[4 \left(\frac{M_*}{M_1}\right)^{3\alpha} 2^{\lambda_3} \Gamma(1+\lambda_3, x_1) \right. \\ &\quad \left. + \left(\frac{M_*}{M_1}\right)^{4\alpha} 2^{\lambda_4} \Gamma(1+\lambda_4, x_1) \right] , \end{aligned} \tag{37}$$

where $\lambda_i = \lambda_0 + i \times 3\alpha/(n+3)$. In the high-mass, high-bias limit we obtain that:

$$T^{1h} \sim b_g^{\frac{3}{2}\frac{n+9}{n+3}} e^{3b_g\,\delta_c/2} \sim \left(P^{1h}\right)^3 . \tag{38}$$

Thus T^{1h} will become a dominant part of the power spectrum covariance matrix in the high bias limit.
The same calculation can be employed generally for the 1-halo term of the $N+1$-th order polyspectrum in the high bias limit, showing that it grows with the scaling $b_g^{\frac{N}{2}\frac{n+9}{n+3}} e^{N b_g\,\delta_c/2} \sim (P^{1h})^N$.

Hence, we conclude that for highly biased tracers not only the power spectrum, but also the higher-order statistics, are increasingly affected by intra-halo statistics, and may become effectively limited not only by the counts of the tracers, but by the counts of the halos as well.

3.2 Sheth-Tormen mass function and a simple HOD

In this Section we still consider, as before, a simplified HOD which does not distinguish between central and satellite galaxies. However, we now consider a cut-off mass for the halo richness, M_c, which is different from the mass scale M_1 (in fact, typically $M_c < M_1$ — see, e.g., Tinker et al. (2008)). Hence, our HOD is:

$$\bar{N}(M) = \left(\frac{M}{M_1}\right)^{\alpha} \theta(M - M_c) . \tag{39}$$

Defining the variable:

$$x = \frac{a}{2}\nu^2 \to \frac{a}{2}\left(\frac{M}{M_*}\right)^{\frac{n+3}{3}} , \tag{40}$$

and the cut-off:

$$x_c = \frac{a}{2}\left(\frac{M_c}{M_*}\right)^{\frac{n+3}{3}} , \tag{41}$$

the calculations of the previous Section can now be performed in basically the same fashion. The number density of halos that can host galaxies is:

$$\begin{aligned} \bar{n}_{h,g} &= \frac{\rho_m}{M_*} \frac{A}{\sqrt{\pi}} \left(\frac{2}{a}\right)^{\lambda_0} \int_{x_c}^{\infty} dx\, x^{\lambda_0} \left[1 + (2x)^{-p}\right] e^{-x} \\ &= \bar{n}_0 \left(\frac{2}{a}\right)^{\lambda_0} \left[\Gamma(1+\lambda_0, x_c) + 2^{-p}\Gamma(1+\lambda_0 - p, x_c)\right] , \end{aligned} \tag{42}$$

where, as previously, $\lambda_0 = -1/2 - 3/(3+n)$, and we have defined $\bar{n}_0 = \rho_m A / M_* \sqrt{\pi}$.

A similar calculation leads to the mean number density of galaxies:

$$\begin{aligned} \bar{n}_g &= \bar{n}_0 \left(\frac{M_*}{M_1}\right)^{\alpha} \left(\frac{2}{a}\right)^{\lambda_1} \\ &\quad \times \left[\Gamma(1+\lambda_1, x_c) + 2^{-p}\Gamma(1+\lambda_1 - p, x_c)\right] , \end{aligned} \tag{43}$$

and the galaxy bias becomes:

$$\begin{aligned} b_g &= 1 - \delta_c^{-1} + \frac{2\delta_c^{-1}}{\Gamma(1+\lambda_1, x_c) + 2^{-p}\Gamma(1+\lambda_1 - p, x_c)} \\ &\quad \times \left[\Gamma(2+\lambda_1, x_c) + 2^{-p}\Gamma(2+\lambda_1 - p, x_c) \right. \\ &\quad \left. + p\, 2^{-p}\Gamma(1+\lambda_1 - p, x_c)\right] . \end{aligned} \tag{44}$$

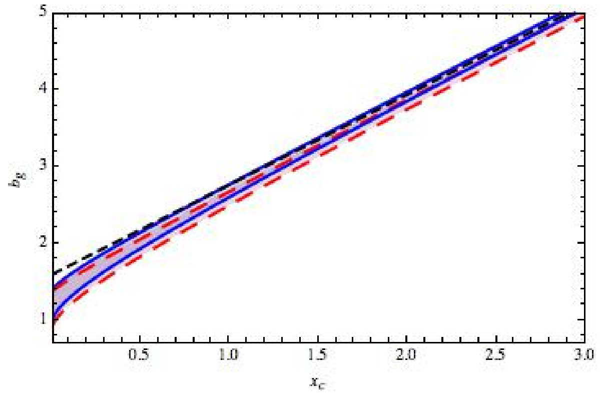

Figure 3. Galaxy bias obtained using the Sheth-Tormen formalism (blue lines and filled region), and in the Press-Schechter formalism (red, long-dashed lines and filled region), as a function of the cut-off scale x_c [see Eq. (41)]. The parameters were allowed to range in the intervals $0.9 < \alpha < 1.1$, and $-2 < n < -1$. The black (short-dashed) line shows the approximation of Eq. (45).

In the limit of $x_c \gg 1$ the galaxy bias can be considerably simplified, in fact:

$$\lim_{x_c=\infty} b_g \to 1 - \delta_c^{-1} + 2\delta_c^{-1} x_c \,, \tag{45}$$

which is basically the approximate expression we obtained in the PS case, where x_1 played the role of the cut-off mass scale. This relationship between the cut-off scale and the bias allows us to write, in the limit of high biases, $x_c \simeq \delta_c(b_g - 1 + \delta_c^{-1})/2$. This turns out to be a fairly good approximation as can be seen from Fig. 3. Notice that we do not expect the model of Eq. (39) to hold for low-biased galaxies, when the small-halo mass limit is critical.

After some algebra, the 1-halo term can be expressed in the same way as was done for the PS case:

$$P^{1h} = q\,\frac{1}{\bar{n}_{h,g}} \,, \tag{46}$$

where:

$$\begin{aligned} q \;=\; & \frac{\Gamma(1+\lambda_0, x_c) + 2^{-p}\Gamma(1+\lambda_0 - p, x_c)}{[\Gamma(1+\lambda_1, x_c) + 2^{-p}\Gamma(1+\lambda_1 - p, x_c)]^2} \\ & \times \left[\Gamma(1+\lambda_2, x_c) + 2^{-p}\Gamma(1+\lambda_2 - p, x_c)\right] \,. \end{aligned} \tag{47}$$

In the limit of $x_c \gg 1$ we can use the series expansion of Eq. (29) to show that, as in the PS case, the prefactor $q \to 1$ [1] . In this limit P^{1h} reduces to the following expression:

$$P^{1h} \simeq \left[\bar{n}_0 \left(\frac{2}{a}\right)^{\lambda_0} x_c^{\lambda_0} \left(1 + 2^{-p} x_c^{-p}\right) e^{-x_c}\right]^{-1} \tag{48}$$

with x_c depending on the bias in the following way:

$$x_c = \frac{\delta_c}{2}(b_g - 1 + \delta_c^{-1}). \tag{49}$$

[1] In this limit, we see from Eq. (46) that the 1-halo term of the power spectrum inherits a dependence on the number density of the halos that contain at least one galaxy. However, the HOD we used in this Section and in the previous one make no distinction between central and satellite galaxies — in fact, we have simply used the typical parametrizations used for satellites. Hence, in this context, $\bar{n}_{h,g}$ should be regarded as the number density of halos containing *more* than one galaxy.

Conversely, in the limit $x_c \ll 1$, we obtain the following scaling for the one-halo term:

$$P^{1h} \simeq \frac{\Gamma(1+\lambda_2) + 2^{-p}\Gamma(1+\lambda_2 - p)}{\bar{n}_0 \left(\frac{2}{a}\right)^{\lambda_0} [\Gamma(1+\lambda_1) + 2^{-p}\Gamma(1+\lambda_1 - p)]^2} \,. \tag{50}$$

Comparing Eq. (36) and Eq. (48), we see that, for high values of the bias, the 1-halo term in the ST model behaves in basically the same way as was found for the PS formalism.

3.3 Semi-analytical model: Tinker mass function and realistic HOD

The analytical approximations of the previous Sections have allowed us to obtain simple expressions for the number densities of galaxies and halos, the bias, and the 1-halo terms, but we made some strong assumptions — in particular, about the simple scaling of halo richness, about the assumption of self-similarity which fixed the scaling of ν with mass, and about the way in which we cut off the halo richness below some given mass scale. Although the final results may have seemed natural and physically sensible, they could have been influenced or even driven by these simplifications.

In this Section we argue that these results are robust. We show this by improving the modeling of the previous Sections in a number of ways: first, we calculate the mass variance $\sigma(M)$ of Eq. (1) from the power spectrum of a vanilla-ΛCDM model; second, we employ the Tinker et al. (2008) mass function and halo bias of Eqs. (22)-(23), which are a slightly better fit to the N-body simulations compared to the PS or ST expressions; and third, we use a class of HODs which is inspired and calibrated by observations (Zheng et al. 2005; Zheng, Coil & Zehavi 2007; Zheng et al. 2009). We also distinguish between central and satellite galaxies — whereas in the preceding Sections we implicitly assumed that all galaxies were satellites.

As for the HOD, we have used the formulas of Eqs. (6)-(7) for the halo richness of central and satellite galaxies. Typical values for these parameters are $M_c \simeq 10^{13.5}\,h^{-1}\,M_\odot$, $M_1 \simeq 10^{14\cdot}\,h^{-1}\,M_\odot$, $\alpha \simeq 0.9$, $\kappa_g \simeq 1.1$, and $\sigma_g \simeq 1$ (Zheng et al. 2009).

In contrast to the previous Sections, where all calculations could be carried out exactly, here we instead compute numerically the galaxy number density of Eq. (9), the bias of Eq. (10), and the 1-halo term of Eq. (12). In this way we can explore basically any point in parameter space, and compute the properties of the galaxy models corresponding to those points.

We allow the parameters to vary in the following ranges, while keeping always $M_c \le M_1$:

$$12.75 < \log_{10} M_c\, h/M_\odot < 14.25 \,, \tag{51}$$
$$13.2 < \log_{10} M_1\, h/M_\odot < 15.0 \,, \tag{52}$$
$$0.85 < \alpha < 1.15 \,, \tag{53}$$
$$0.85 < \sigma_g < 1.15 \,, \tag{54}$$
$$1.0 < \kappa_g < 1.3 \,. \tag{55}$$

The results for the 1-halo term of the power spectrum are shown in the top panel of Fig. 4. We have split the different HOD models in four groups, according to the number densities of galaxies. From the bottom, the horizontal shaded areas correspond to HODs whose ranges of $\bar{n}_g^{-1}$ fall in the intervals $10^{-L+0.15} \geq \bar{n}_g\,(h^3\,\mathrm{Mpc}^{-3}) \geq 10^{-L-0.15}$, for $L = 3.3$, 3.6, 3.9, and 4.2 . The values of P^{1h} for models in those four groups are shown as points of the same colors as the shaded areas, from lower left to upper right, respectively. The dashed black line is the power-law $b_g^{4.5}$.

We saw in Sections 3.1 and 3.2 that the one-halo term evolves like a power-law in b_g for intermediate values of the galaxy bias. This is again what we observe here: the asymptotic behavior of the one-halo follows a steep power-law as a function of galaxy bias. The growth of the one-halo term is constrained by the requirement that $M_c \leq M_1$, which limits the number of galaxies in halos, and imposes an upper limit on the bias and the one-halo term. If we relax this physical requirement, the power-law evolution of the one-halo term continues at higher bias.

The results obtained in Sections 3.1 and 3.2 were derived under the assumption that all galaxies are of the "satellite" type — an approximation that we did not use here. For highly biased tracers the 1-halo term can be comparable to Poisson shot noise, which shows that the "central" galaxies are less relevant in that limit, providing a motivation for that approximation in Sections 3.1 and 3.2. Conversely, the fact that P^{1h} drops well below the level of galaxy shot noise for low values of the bias shows that, for such types of objects, the central galaxy plays an important role, as many (or most) halos host a single central galaxy.

In the bottom panel of Fig. 4 we show the results for the 1-halo term of the trispectrum of Eq. (14), in the limit $k \to 0$, $k' \to 0$, for the same range of HOD parameters used in the top panel. Again, we separate the models in groups, according to the number density of galaxies, and the horizontal shaded areas denote the different values of n_g^{-3} for each group. The dashed line is the power-law $b_g^{13.5}$.

As argued above, the 1-halo term of the trispectrum also scales rapidly with bias, approximately as $(P^{1h})^3$. In Fig. 5 we show the 1-halo term of the trispectrum [Eq. (14)] against the 1-halo term of the power spectrum. The dashed line indicates the scaling $(P^{1h})^{2.5}$.

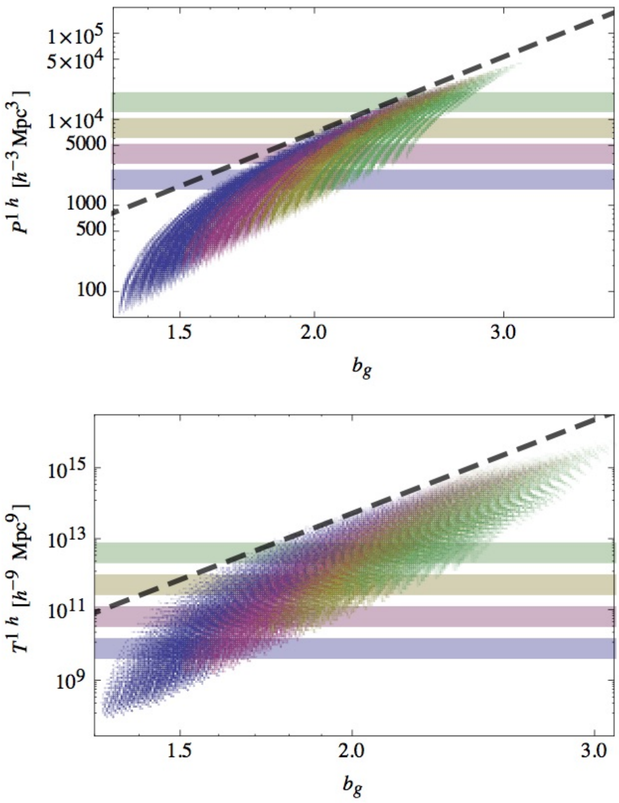

Figure 4. Top panel: 1-halo term in the HOD of Eqs. (6)-(7). The models were split according to the number density of galaxies. From left to right, and from the bottom up, the models shown have $10^{-3.15} \geq \bar{n}_g \geq 10^{-3.45}$, $10^{-3.45} \geq \bar{n}_g \geq 10^{-3.75}$, $10^{-3.75} \geq \bar{n}_g \geq 10^{-4.05}$, and $10^{-4.05} \geq \bar{n}_g \geq 10^{-4.35}$. In each case, the horizontal shaded area marks the corresponding range of $1/\bar{n}_g$. The dashed black line is the power-law $b_g^{4.5}$. The stripes seen mostly in the lower right corner are just an artifact of the grid we used to explore the HOD parameter space. Bottom panel: 1-halo term of the trispectrum for the same class of HODs. The dashed black line is the power-law $b_g^{13.5}$. The horizontal shaded areas mark the corresponding ranges of $1/\bar{n}_g^3$.

3.4 Simulations

We further test the results from the previous sections in a fully numerical set-up, by using a catalog of halos from the DEUS simulations [2] (Alimi et al. 2010; Rasera et al. 2010; Courtin et al. 2011). We use halos detected with the Friends-of-Friends algorithm in a box of 648 h^{-1} Mpc, containing 1024^3 dark matter particles, in a ΛCDM cosmology in agreement with WMAP5 (Komatsu et al. 2009). We should note that the DEUS mass function is very well fit by the Tinker mass function, and that the DEUS halo bias is also well fit by the Tinker halo bias.

We populate the halos using the HOD formalism presented in Eqs. (6) and (7), with fixed parameters $\alpha = 0.9$, $\sigma_g = 1.0$ and $\kappa_g = 1.1$. The M_c and M_1 parameters are allowed to vary in the ranges given in Eqs. (51)-(52).

The number N_c of central galaxies is either 0 or 1, and is drawn from a nearest-integer uniform distribution with mean $\bar{N}_c$. For halos containing a central galaxy, the number of satellite galaxies is then drawn from a Poisson distribution with mean $\tilde{N}_s$ (since we are taking the $k \to 0$ limit for the 1-halo term, it is irrelevant where in the halo those satellite galaxies are placed). Obviously, halos that do not contain a central galaxy have no satellite galaxies.

With the DEUS halo catalog, and the HOD implementation described above, expressions such as that for the number density of galaxies become:

$$\begin{aligned} \bar{n}_g &= \int_{M_1}^{\infty} d\ln M\, \frac{d\bar{n}_h}{d\ln M} \times \bar{N}(M) \qquad (56) \\ &\longrightarrow \frac{1}{V}\sum_h \{N_c[M(h)] + N_s[M(h)]\} \\ &= \frac{1}{V}\sum_M N_h(M)\,[\bar{N}_c(M) + \bar{N}_s(M)]\,, \end{aligned}$$

where V is the volume of the simulation. In order to compute galaxy bias, for simplicity we employ the Tinker bias, Eq. (23), in Eq. (10).

The resulting scaling between the one-halo term and the

[2] http://www.deus-consortium.org

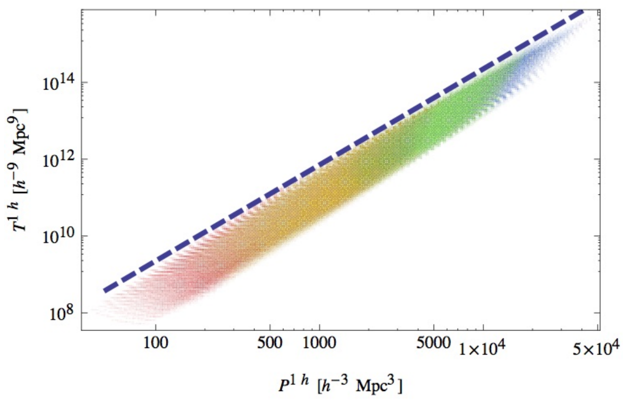

Figure 5. 1-halo term of the trispectrum plotted against the 1-halo term of the power spectrum, for the HOD of Eqs. (6)-(7). The dashed black line is the power-law $(P^{1h})^{2.5}$. The models were split according to bias: from lower left to upper right, the different colors indicate models with $1.0 \le b_g \le 1.5$, $1.5 \le b_g \le 2.0$, $2.0 \le b_g \le 2.5$, and $2.5 \le b_g \le 3.0$.

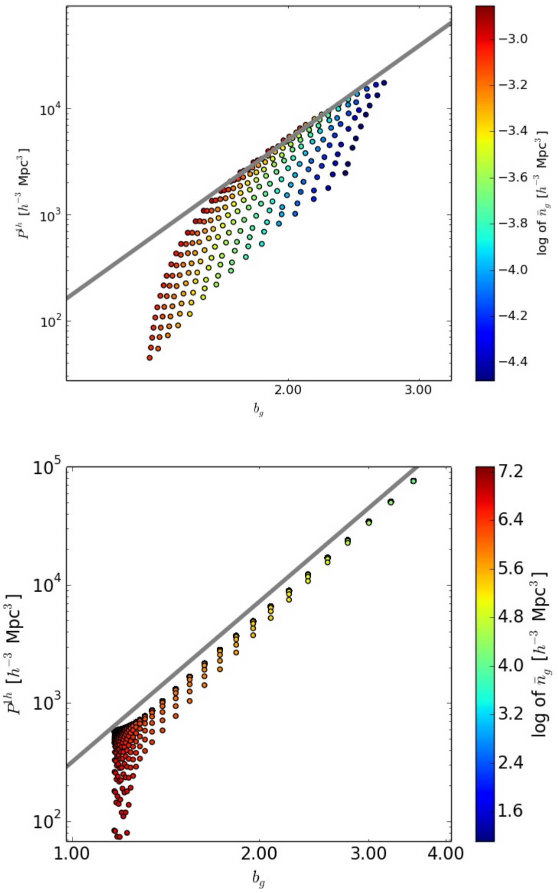

Figure 6. One-halo term and galaxy bias obtained from the DEUS simulated halo catalog populated with the HOD of Eqs. (6)-(7) (top panel), and with the test HOD of Eq. (57) (bottom panel). In the top panel, the grey line shows the scaling b_g^5, while in the bottom panel the scaling is $b_g^{4.5}$.

galaxy bias is shown in the top panel of Fig. 6. The same type of scaling found in the previous sections appears here — the grey line indicates the power-law $P^{1h} \propto b_g^5$. In order to check whether this scaling is sensitive to the precise form of the HOD used, we also test a different HOD prescription for which:

$$\bar{N}_g \propto \log \frac{M}{M_c} \text{ for } M > M_c. \tag{57}$$

The number of galaxies in each halo is drawn from a Poisson distribution with mean given by the formula above. The scaling obtained in this case between the one-halo term and the galaxy bias is shown on the bottom panel of Fig. 6. The grey line now follows $b_g^{4.5}$, a scaling very similar to the one found in the previous cases.

As is the case in the original HOD of the previous sections, in this alternative HOD prescription the richness is an increasing function of halo mass. We also tested HOD models where the richness becomes constant, or even decreases, with increasing halo mass, and in those cases we do not recover the same type of scaling between bias and the one-halo term of the power spectrum. However, we do not consider this to be a limitation of our study, as we expect realistic HODs to display an average number of galaxies monotonically increasing with halo mass.

4 DISCUSSION

We have shown that, when the galaxy bias is high enough ($b_g \gtrsim 3$), the 1-halo term of the power spectrum grows faster as a function of bias than the 2-halo term. We also showed that the 1-halo term of the trispectrum grows much faster than the 4-halo term. We argue that the 1-halo terms of all the N-polyspectra scale faster than the N-halo terms of those polyspectra.

We interpret these results in the following way. Galaxy bias provides an intuitive physical interpretation of the way in which the visible matter distribution is related to the underlying DM distribution. Given a Gaussian field δ_G, taken from a distribution whose variance (in Fourier space) is basically the matter power spectrum, the density contrast of a biased tracer on a grid of finite-volume cells can be approximated by a lognormal field, $\delta_g = \exp[b_g\delta_G - b_g^2\sigma_G^2/2] - 1$, where b_g is the bias of the tracer, and σ_G^2 is the variance of the Gaussian field on the volume of the cell of the grid (Coles & Jones 1990). As the bias increases, the number of particles found in the density peaks grow very fast (Bardeen et al. 1986) — exponentially, in the lognormal model — while most of the space is emptied.

In terms of the Halo Model, we can vary the HOD parameters in such a way that the mean number density is kept fixed while the bias increases. For highly biased galaxies we expect to find more objects concentrated in fewer halos. This implies that, for very high values of the bias, the galaxy 2-point statistics can get a large contribution from the statistics of halos hosting two or more galaxies. This argument extends to all the N-point statistics: in the high-bias limit there will be many galaxies inside the same few halos, which means that all the 1-halo terms of the N-point statistics will become increasingly important.

In Section 3.1, within the Press & Schechter (1974) formalism, we used very simple formulas for the halo richness and for the scaling of the mass variance (and peak height), to show that the 1-halo term of the power spectrum grows very fast with bias. A more refined analytical calculation, done in Section 3.2 using the Sheth & Tormen (1999) framework, shows basically the same scaling. In Section 3.3 we employed the Tinker et al. (2008) mass function, realistic HODs, and an exact computation of the mass variance in ΛCDM models, and confirmed that the 1-halo term of the power spectrum scales at least as fast as $P^{1h} \sim b_g^{4-5}$. Similarly, we showed that the 1-halo term of the trispectrum scales as fast as $T^{1h} \sim b_g^{12-15}$. Finally, in Section 3.4 we used a halo catalog derived from the DEUS simulation, and two different kinds of HODs, and again obtained the same scaling laws.

The fact that simple analytical arguments show the correct scaling of the 1-halo terms with bias is a hint that these results should be related to basic properties of Gaussian fields and the matter power spectrum. In fact, tracers of different biases effectively probe different scales in the power spectrum: higher/lower masses (and higher/lower biases) are related to larger/smaller scales. Since the matter power spectrum has a power index that ranges between $n \simeq -1$ at large scales, to $n \simeq -2$ at small scales, the power index which is relevant for the halo masses typical of a certain type of galaxy is also an indicator of the bias of that galaxy. Conversely, bias also tells us how galaxies are distributed among the dark matter halos, and about the typical peak height which corresponds to a galaxy with that bias. In particular, a higher bias implies that galaxies will be more concentrated on fewer halos, enhancing the 1-halo terms. Since all these properties can be traced back to the slope of the power spectrum, it is not surprising to find that different types of galaxies present the same scaling of the 1-halo term with bias.

Since the 1-halo terms are constant on large scales, for cosmological surveys that cannot resolve the inner structure of halos, these terms enter effectively as additional sources of noise and covariance. Conversely, very accurate and complete surveys will be able to detect much better the amplitudes and scale dependences of the 1-halo terms when the bias is sufficiently high, implying better constraints on HOD parameters.

In particular, cosmological surveys targeting highly-biased objects could be severely impacted by the effects of the statistics of counts of the halos hosting those objects. Measurements of the power spectrum from these surveys should take into account not only the higher effective shot noise coming from the 1-halo term of the power spectrum, but also the additional contribution to the power spectrum covariance coming from the 1-halo term of the trispectrum. Similarly, measurements of the bispectrum which employ highly biased tracers should ensure that the relevant 1-halo terms are properly taken into account.

Finally, although we worked at $z = 0$, it would be interesting to find out what happens at high redshifts. On the one hand, the bias of a given population of tracers is typically increasing as a function of redshift; but on the other hand, linear theory should become a better approximation, which means that the 1-halo term should be less important. Therefore, at higher redshifts the form of the scaling of the 1-halo term should depend sensitively not only on the amplitude of the power spectrum, but also on the evolution of the HOD parameters.

Acknowledgements

We would like to thank Marcello Musso and Ravi Sheth for useful discussions. We acknowledge support from the DIM ACAV of the Region Île-de-France for the storage of the DEUS data. We would also like to thank FAPESP, CAPES, CNPq, and the University of São Paulo's *NAP LabCosmos* for financial support. IB acknowledges support from FAPESP through the grant 2013/21069-9, and FL acknowledges support from FAPESP through grants 2011/11973 and 2013/19936-6.

References

Abbott, T. *et al.*, 2005, astro-ph/0510346
Abell, P., *et al.*, 2009, 0912.0201
Abramo, L. R., *et al.*, 2012, MNRAS, 423, 335
Adelman-McCarthy, J. K., *et al.*, 2008a, VizieR Online Data Catalog, 2282, 0
Adelman-McCarthy, J. K., *et al.*, 2008b, ApJS, 175, 297
Alimi, J.-M., Füzfa, A., Boucher, V, Rasera, Y., Courtin, J., Corasaniti, P. S., 2010, MNRAS, 401, 775
Anderson, L., *et al.*, 2012, MNRAS, 427, 3435
Anderson, L., *et al.*, 2014, MNRAS, 439, 83
Bardeen, J. M., Bond, J. R., Kaiser, N., Szalay, A. S., 1986, ApJ, 304, 15
Bartolo, N., Komatsu, E., Matarrese, S., & Riotto, A., 2004, Phys. Rept., 402, 103
Benson, A. J., Cole, S., Frenk, C. S, Baugh, C. M., Lacey, C. G., MNRAS, 311, 793-808
Benítez, N., *et al.*, 2009, ApJ, 691, 241
Benítez, N., *et al.*, 2014, 1403.5237
Berlind, A. A., Weinberg, D. H., 2002, ApJ 575, 587
BigBOSS: http://bigboss.lbl.gov/ .
Blake, C., *et al.*, 2011, MNRAS, 415, 2876
BOSS: http://cosmology.lbl.gov/boss/ .
Carron, J., 2011, ApJ, 738, 86
Carron, J., 2012, Phys. Rev. Lett., 108, 7
Carron, J., Neyrinck, M. C., 2012, ApJ, 750, 1
Carron, J., 2014, 1406.6095
Cen, R., Safarzadeh, M., 2015, ApJL, 798, 38
Chatterjee, S., Nguyen, M. L., Myers, A. D., Zheng, Z., 2013, ApJ 779, 147
Cole, S., *et al.*, 2005, MNRAS, 362, 505
Coles, P., Jones, B., 1990, MNRAS, 248, 1
Cooray, A., Sheth, R., 2002, Phys. Rept., 372, 1
Courtin, J., Rasera, Y., Alimi, J.-M., Corasaniti, P. S., Boucher, V., Füzfa, A., 2011, MNRAS, 410, 1911
Croom, S., *et al.*, 2005, MNRAS, 356, 415
da Ângela, J., *et al.*, 2005, MNRAS, 360, 1040
Dalal, N., Doré, O., Huterer, D., Shirokov, A., 2008, Phys. Rev., D77, 123514
Ellis, R., Takada, M., *et al.*, The PFS Team, 1206.0737
Fry, J., Gaztañaga, E., 1993, ApJ, 413, 447
Kauffmann, G., White, S. D. M., Guiderdoni, B., 1993, MNRAS, 264, 201
Kauffmann, G., Colberg, J. M., Diaferio, A., White, S. D. M. 1999, MNRAS, 303, 188

Kayo, I., Oguri, M., 2012, MNRAS, 424, 1363
Komatso, E., et al., 2009, ApJS, 180, 330
Kravtsov, A. V., Berlind, A. A., Wechsler, R. H., Klypin, A. A., GottlÃ¶ber, S., Allgood, B., Primack, J. R., 2003, ApJ, 609, 35
Hill, G. J., *et al.*, 2008, in "Panoramic Views of the Universe", ASP Conf. Series, 399, 115
Leistedt, B., Peiris, H. V., Mortlock, D. J., Benoit-LÃ©vy, A., Pontzen, A., 2013, MNRAS, 435, 1857
Leistedt, B., Peiris, H. V., 2014, MNRAS, 444, 2
Linder, E., 2005, Phys. Rev., D72, 043529
Ma, C.-P., Fry, J. N., 2000, ApJ, 543, 503
Maldacena, J., 2003, JHEP, 5
Martinez, V., Saar, E., 2001, "Statistics of the Galaxy Distribution" (CRC Press, 2001)
Mo, H., White, S. D. M., 1995, MNRAS, 282, 347
Navarro, J. F. and Frenk, C. S., White, S. D. M., 1995, MNRAS, 275, 56
Navarro, J. F. and Frenk, C. S. and White, S. D. M., 1997, ApJ, 490, 483
PAN-STARRS: http://pan-starrs.ifa.hawaii.edu/public/
Planck Collaboration, 2015, 1502.01589
Piscionere, J. A., Berlind, A. A., McBride, C. K., Scoccimarro, R., 2014, 1407.6740
Porciani, C., Magliocchetti, M., Norberg, P. 2004, MNRAS, 355, 1010
Press, W. H., Schechter, P., 1974, ApJ, 187, 425
Rasera, Y., Alimi, J.-M., Courtin, J., Roy, F., Corasaniti, P.-S., Füzfa, A., Boucher, V., 2010, INVISIBLE UNIVERSE: Proceedings of the Conference. AIP Conference Proceedings, 1241, 1134-1139
Richardson, J., Zheng, Z., Chatterjee, S., Nagai, D., Shen, Y., 2012, ApJ, 755, 30
Ross, A., *et al.*, 2009, ApJ, 697, 1634
Scoville, N., *et al.*, 2007, ApJS, 172, 1
Seljak, U., 2000, MNRAS, 318, 203
Seljak, U., 2009, Phys. Rev. Lett., 102, 021302
Shen, Y., et al., 2007, AJ, 133, 2222
Shen, Y., et al., 2010, ApJ, 719, 2
Shen, Y., et al., 2013, ApJ, 778, 98
Sheth, R. K.,Mo, H. J., Tormen, G., 2001, MNRAS, 323, 1
Sheth, R. K., Tormen, G., 1999, MNRAS, 308, 119
Slosar, A., et al., 2013, JCAP, 04, 026
Springel, V., et al., 2005, Nature, 435, 629
SUMIRE: http://sumire.ipmu.jp/en/
Thacker, C., et al., 2013, ApJ, 768, 58
Tinker, J., Kravtsov, A. V., Klypin, A., Abazajian, K., Warren, M., Yepes, G., Gottlöber, S., Holz, D. E., 2008, ApJ, 688, 709
Tinker, J. L. and Robertson, B. E. and Kravtsov, A. V. and Klypin, A. and Warren, M. S. and Yepes, G. and Gottlöber, S., 2010, ApJ, 724, 878
Verde, L., Wang, L., Heavens, A. F., Kamionkowski, M., 2000, MNRAS, 313, 141
Wake, D. A., Croom, S. M., Sadler, E. M., Johnston, H. M., 2008, MNRAS, 391, 1674
Watson, D. F., Berlind, A. A., McBride, C. K., Masjedi, M., 2010, ApJ, 709, 115
Berlind, A. A., Weinberg, D. H., 2002, ApJ, 575, 587
White, S., Frenk, C., 1991, ApJ, 379, 52
York, D. G., *et al.*, 2000, AJ, 120, 1579
Zentner, A. R., Hearin, A. P., van den Bosch, F. C., 2014, MNRAS, 443, 3044
Zheng, Z., *et al.*, 2005, ApJ, 633, 791
Zheng, Z., Coil, A., Zehavi, I., 2007, ApJ, 667, 760
Zheng, Z., Zehavi, I., Eisenstein, D. J., Weinberg, D. H., Jing, Y. P., 2009, ApJ, 707, 554